manuscript No.
(will be inserted by the editor)

Statistical Physics Model of Seismic Activation Preceding a Major Earthquake

Daniel S. Brox - Alumni Caltech:
brox@alumni.caltech.edu

Received: date / Accepted: date

Abstract Starting from earthquake fault dynamic equations, a correspondence between earthquake occurrence statistics in a seismic region before a major earthquake and eigenvalue statistics of a differential operator whose bound state eigenfunctions characterize the distribution of stress in the seismic region is derived. Modelling these eigenvalue statistics with a 2D Coulomb Gas statistical physics model, previously reported deviation of seismic activation earthquake occurence statistics from Gutenberg-Richter statistics in time intervals preceding the major earthquake is derived. It is also explained how statistical physics modelling predicts a finite dimensional nonlinear dynamic system describes real time velocity model evolution in the region undergoing seismic activation, and how this prediction can be tested experimentally.

Keywords seismic activation · statistical physics · geodynamics · signal processing

1 Introduction

An increase in the number of intermediate sized earthquakes (M $>$ 3.5) in a seismic region preceding the occurrence of a major earthquake (7 $<$ M $<$ 8), referred to as seismic activation, has been observed to occur before many major earthquakes [6]. For example, seismic activation was observed in a geographic region spanning $21^\circ N - 26^\circ N \times 119^\circ E - 123^\circ E$ for a period of time between 1991 and 1999 preceding the magnitude 7.6 Chi-Chi earthquake [11]. Figure 1 shows a schematic plot of the cumulative distribution of earthquakes of different magnitudes in a region undergoing seismic activation in two different time intervals of equal duration preceding occurrence of a major earthquake at time $\tau = \tau_0$. In this figure, τ is a real time parameter, and τ_0 is the characteristic time of major earthquake recurrence assuming an earthquake of similar magnitude occurred in the same region at $\tau = 0$ [31]. Importantly, the cumulative distribution of earthquakes in a time interval of fixed width

Address(es) of author(s) should be given

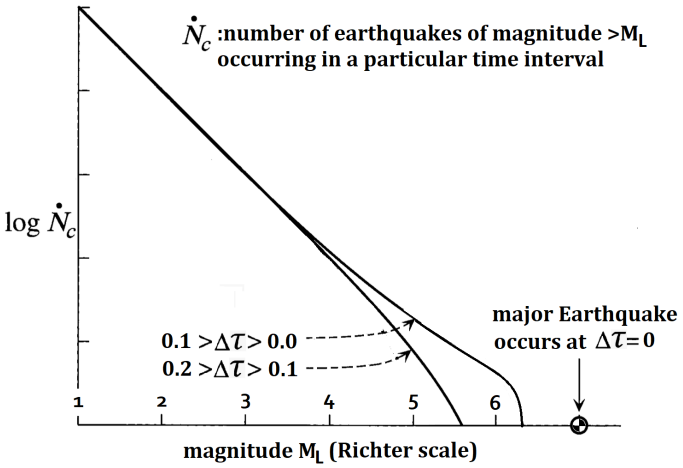

Fig. 1 Plot of the cumulative distribution of earthquakes of different magnitudes in a seismic zone in two different time intervals of equal width preceding occurrence of a major earthquake at $\Delta\tau = \tau_0 - \tau = 0$ [31].

increasingly deviates away from a Gutenberg-Richter linear log-magnitude plot as the end of the time interval approaches τ_0.

As a means of predicting the time $\tau = \tau_0$ at which a major earthquake preceded by seismic activation occurs, it has been hypothesized that the average seismic moment $\langle \mathrm{M} \rangle_\tau$ of earthquakes occuring in intervals of time $(\tau, \tau + \Delta\tau)$ preceding a major earthquake obeys an inverse power of remaining time to failure law:

$$\langle \mathrm{M} \rangle_\tau \propto \frac{1}{(\tau_0 - \tau)^{\gamma_1}} \tag{1}$$

and that as a result, the cumulative Benioff strain $\mathscr{C}(\tau)$, defined as:

$$\mathscr{C}(\tau) = \sum_{i=1}^{n(\tau)} \mathrm{M}_{0,\mathrm{i}}^{1/2}, \tag{2}$$

where $\mathrm{M}_{0,i}$ is the seismic moment of the i^{th} earthquake in the region starting from a time $\tau = 0$ preceding the major earthquake, and $n(\tau)$ is the number of earthquakes occurring in the region up to time τ, satisfies:

$$\mathscr{C}(\tau) = a - b(\tau_0 - \tau)^{\gamma_2}, \ \gamma_2 = 1 - \gamma_1/2. \tag{3}$$

Notably, the exponent selection of $1/2$ in equation (2) is not necessary to derive formula (3) with a different arithmetic relation between γ_1 and γ_2, but appears to have been commonly selected by previous researchers based on resulting predictions of major earthquake occurrence time when formula (3) is fit to real seismic data [27]. It is also noted that when a fit to real seismic data is performed, a value $\gamma_2 \approx 0.3$ is typical [6].

A mathematical model of seismic activation based on damage mechanics of earthquake faults has been put forth to derive equation (3) with a value $\gamma_2 = 1/3$ [4]. In

this derivation, the occurrence of seismic activation earthquakes progressively decreases the average shear modulus of unruptured fault material in the seismic region where subsequent seismic activation earthquakes occur, and the result $\gamma_2 = 1/3$ is determined by a Boltzman kinetic type description of how ruptured faults of different lengths at different positional locations propagate and join together [39].

In addition to the damage mechanics model of seismic activation, an empirical model of seismic activation using statistical physics known as the Critical Point (CP) model has been put forth to derive equation (3) with a value $\gamma_2 = 1/4$ [31]. In this derivation, the inverse power of remaining time to failure law:

$$\langle \mathrm{M} \rangle_\tau \propto \frac{1}{(\tau_0 - \tau)^{3/2}} \tag{4}$$

is asserted based on identifying the mean rupture length $\mathscr{L}(\tau)$ of earthquakes occuring at time τ with the correlation length of a statistical physical system described by Ginzburg-Landau mean field theory with a temperature parameter depending on τ, whereby:

$$\mathscr{L}(\tau) \propto \frac{1}{(\tau_0 - \tau)^{1/2}}, \tag{5}$$

and relation (4) follows from assuming $\langle \mathrm{M} \rangle_\tau \propto \mathscr{L}(\tau)^3$ when fault material shear modulus is constant in the seismic activation region [32]. Importantly, previous work has not explained why it is physically reasonable to describe statistics of seismic activation with thermal equilibrium statistical physics formalism, or what predictions other than time of major earthquake occurrence are possible with such models. Therefore, the objective of this article is to advance the detailed mathematical description of the correspondence between nonlinear differential equation modelling and statistical physics modelling of seismic activation in a way that advances testing of model predictions against real seismic measurements.

The outline of the article is as follows. Section 2 introduces a sine-Gordon equation modelling earthquake fault dynamics during seismic activation and explains how inverse scattering theory of this equation implies a relation between statistics of earthquake occurrence during seismic activation and the eigenvalue statistics of a differential operator whose bound state eigenfunctions characterize the distribution of stress in the seismic region. Section 3 uses this relation to model eigenvalue statistics with a 2D Coulomb Gas statistical physics model, and explains how this model accounts for deviation of earthquake occurrence statistics from Gutenberg-Richter statistics during seismic activation. Section 4 concludes by commenting on how the 2D Coulomb Gas statistical physics model implies the phase space dimension of a nonlinear dynamical system characterizing real time velocity model evolution in the seismic activation region is finite, and how this implication can be tested against real seismic measurements.

2 Methods

2.1 1D Fault Dynamics Inverse Scattering Theory

In 1+1 spacetime dimensions, the differential equation:

$$A\partial_\tau^2 U(\tau,z) + B\partial_\tau U(\tau,z) - C\partial_z^2 U(\tau,z) = -\sin(U(\tau,z)/D). \tag{6}$$

has been used to model migration of earthquake hypocentres along earthquake faults in seismic regions over periods of time during which multiple earthquakes occur, and is here put forth as a model of seismic activation [8]. In this equation, τ is real time, z coordinates a direction of earthquake hypocenter migration along an earthquake fault, $U(\tau,z)$ is the local displacement of elastic material across the earthquake fault, $A\partial_\tau^2 U(\tau,z)$ is the local inertial force acting on the fault material, $B\partial_z^2 U(\tau,z)$ is the local elastic restoring force acting on the fault material, and $C\partial_\tau U(\tau,z)$ and $\sin(U(\tau,z)/D)$ are local frictional force acting on the fault material attributed to periodic contact of the material with tectonic plates on either side of the fault. If the earthquake fault material has constant height h and shear modulus μ along the fault, a solution to equation (6) can be interpreted to describe propagation of shear stress along the z-axis, which in this 1 dimensional model is identified with the both the direction of hypocentre migration and the direction of all earthquake slip vectors.

Restricting focus to the case $C = 0$, with rescaling of τ, z, and $U(\tau,z)$, each of the constants A, B, and D in equation (5) can be set to 1. With this rescaling, and definition of the matrices:

$$M = \begin{bmatrix} -i\omega & -\frac{1}{2}U_z(\tau,z) \\ \frac{1}{2}U_z(\tau,z) & i\omega \end{bmatrix}, \tag{7}$$

$$N = \frac{i}{4\omega}\begin{bmatrix} \cos U(\tau,z) & \sin U(\tau,z) \\ \sin U(\tau,z) & -\cos U(\tau,z) \end{bmatrix}, \tag{8}$$

for an arbitary complex number ω, the equation:

$$M_\tau - N_z + MN - NM = 0, \tag{9}$$

is equivalent to equation (5) [22]. Moreover, introduction of the matrix operator M permits introduction of the associated seismic wave scattering problem:

$$\frac{\partial}{\partial z}\begin{bmatrix} \Psi_1(\tau,z) \\ \Psi_2(\tau,z) \end{bmatrix} = M\begin{bmatrix} \Psi_1(\tau,z) \\ \Psi_2(\tau,z) \end{bmatrix}, \tag{10}$$

in which, according to the inverse scattering method, τ is an auxillary parameter, and oscillatory dependence $e^{-i\omega t}$ of the incoming and outgoing scattered waves on a scattering time parameter t has been implicitly assumed in the definitions of M and N.

Upon definition of scattering problem (10), the inverse scattering method proceeds by determining an infinite set of its left and right scattering (i.e. Jost) solutions

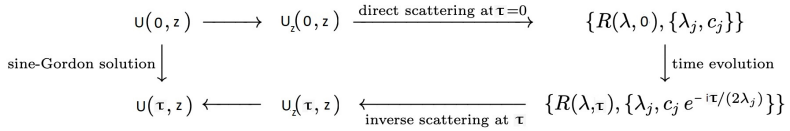

Fig. 2 Schematic of diagram of inverse scattering method applied to solve the sine-Gordon equation [2]. Real time τ evolution of the scattering data determines a solution to the sine-Gordon equation upon application of an inverse scattering transform.

$\Psi_{\lambda,L}(\tau,z)$ and $\Psi_{\lambda,R}(\tau,z)$, indexed in this case by complex wave numbers $\lambda=\omega$, with asymptotics [2]:

$$\Psi_{\lambda,L}(\tau,z)=\begin{bmatrix}0\\ e^{i\lambda z}\end{bmatrix},\ z\to\infty \tag{11}$$

$$\Psi_{\lambda,L}(\tau,z)=\begin{bmatrix}\frac{L(\lambda,\tau)e^{-i\lambda z}}{T(\lambda)}\\ \frac{e^{i\lambda z}}{T(\lambda)}\end{bmatrix},\ z\to-\infty, \tag{12}$$

and:

$$\Psi_{\lambda,R}(\tau,z)=\begin{bmatrix}e^{-i\lambda z}\\ 0\end{bmatrix},\ z\to-\infty \tag{13}$$

$$\Psi_{\lambda,R}(\tau,z)=\begin{bmatrix}\frac{e^{-i\lambda z}}{T(\lambda)}\\ \frac{R(\lambda,\tau)e^{i\lambda z}}{T(\lambda)}\end{bmatrix},\ z\to\infty. \tag{14}$$

Next, the effect of real time τ evolution of the Jost functions is calculated in terms of τ-variation of the reflection coefficients $R(\lambda,\tau)$ and a finite set of complex numbers $\{c_j\}$ associated with complex wave numbers $\{\lambda_j\}$ of bound state solutions to linear system (10). Finally, the real time evolved sine-Gordon equation solution $U(\tau,z)$ is determined by applying an inverse scattering transform to the real time evolved scattering data as indicated in Figure 2. Note that according to 1D scattering theory, scattering bound states are in correspondence with zeroes of the function $T(\lambda)$, while resonant scattering states are in correspondence with zeros of the reflection coefficients $R(\lambda,\tau)$ and $L(\lambda,\tau)$ at fixed values of τ. Also note that in general the bound and resonant state $\{\lambda_j\}$ values have non-zero imaginary components, and are located symmetrically with respect to the imaginary axis in the complex λ-plane.

To clarify physical interpretation of the Jost functions used by the inverse scattering method, observe that for a potential function $V(z)$ compactly supported along the z-axis, the operator:

$$-B\partial_z^2+V(z), \tag{15}$$

has infinitely many resonant state eigenfunctions $\Psi(z)$ satisfying the elastic wave equation:

$$-B\partial_z^2\Psi(z)+V(z)\Psi(z)=E\Psi(z), \tag{16}$$

and finitely many bound state eigenfunctions $\Psi_j(z)$ with negative real eigenvalues $E_j = \omega_j^2 < 0$. Consequently, a solution $\bar{\Psi}(t,\tau,z)$ to the linear seismic wave equation:

$$\partial_t^2 \bar{\Psi}(t,\tau,z) - B(\tau)\partial_z^2 \bar{\Psi}(t,\tau,z) + V(\tau,z)\bar{\Psi}(t,\tau,z) = 0. \tag{17}$$

in which the auxillary seismic wave scattering time parameter t is introduced, and τ tracks parameter changes associated with seismic activation, has a resonant scattering expansion of the form:

$$\bar{\Psi}(t,\tau,z) = \sum_{j=1}^{N} e^{t\sqrt{-E_j}} a_j \Psi_{j,a}(\tau,z) + e^{-t\sqrt{-E_j}} b_j \Psi_{j,b}(\tau,z) + \sum_{\omega \; resonant} e^{-it\omega} c_\omega \Psi_\omega(\tau,z), \tag{18}$$

in which exponential growth and decay of the bound states determines the geometric form of an elastic perturbation $\bar{\Psi}(t,\tau,z)$ over time.

For example, if $V(\tau,z)$ is a potential well of depth $V_0 > 0$ which is independent of τ, nonzero for $|z| \leq L$, and zero elsewhere, there exist finitely many bound state eigenfunctions $\Psi_j(z)$ which decay exponentially with increasing $|z|$:

$$\Psi_j(z) \propto e^{-k_j|z|}, \; |z| \to \infty \tag{19}$$

for a discrete set of spatial decay constants:

$$k_j = \sqrt{-E_j/B}, \tag{20}$$

whose inverse values determine characteristic length scales at which unstable growth of fault material displacement may occur across the earthquake fault. Figure 3 shows a plot of resonant and bound state frequency locations for 3 situations in which $-\frac{1}{B}V(z)$ is a square well potential of increasing width and fixed height.

2.2 3D Fault Dynamics to Statistical Physics

In 3 spatial dimensions, the previous discussion of inverse scattering in 1 spatial dimension can be generalized with reference to the theory of elastodynamic Green's functions [41]. More specifically, given an elastodynamic Green's function on an elastic 3D half space with spatially varying elastic impedance, the Fourier transform of this Green's function has poles at complex resonant frequencies $\omega = \omega_j$ identifying elastodynamic resonant scattering states. Moreover, the residues $\{c_j\}$ of the Fourier transformed Green's function at the pole locations $\{\omega_j\}$, together with the pole locations, constitute a 3D generalization of inverse scattering data. Therefore, allowing both the pole locations and associated residues to depend on τ, real time evolution of 3D scattering data is defined in such a way that it is necessarily in correspondence with real time evolution of the elastic impedance of the half space.

Without addressing appropriate mathematical definition of differential operators M and N for describing τ-dependent elastic scattering in a 3D half space and holographic real time evolution of 3D scattering data, it remains possible to conjecture

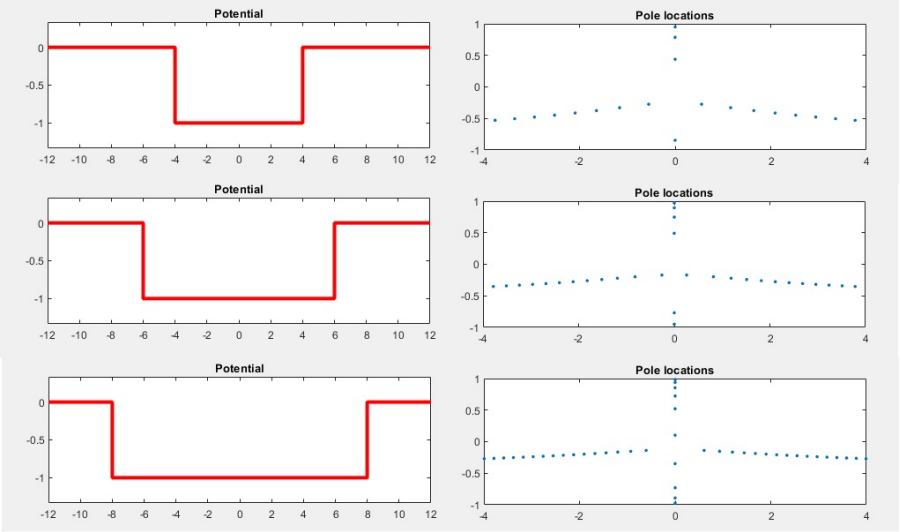

Fig. 3 Plots of resonant frequency and bound state frequency locations for 3 square well potentials of increasing width.

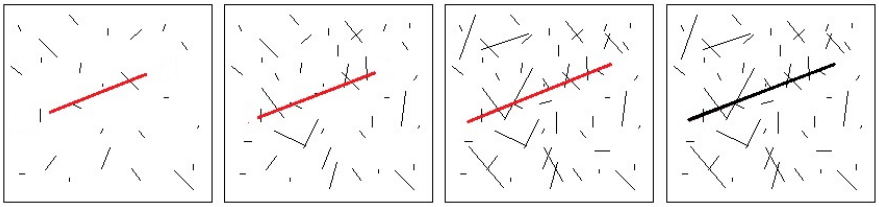

Fig. 4 Schematic illustration of seismic activation in a 2D geometry at four different times τ in which each black line represents an earthquake fault along which rupture has occured, and each red line represents an earthquake fault along which shear stress is increasing prior to rupture at $\tau = \tau_0$.

how statistical properties of 3D scattering data descriptive of seismic activation depend on τ by applying previous work on elastic scattering theory and statistical physics models of seismic activation. To this end, Figure 4 illustrates a random fracture network model of a seismic activation region at 4 different times τ, whereby occurrence of seismic activation earthquakes and the major earthquake at time $\tau = \tau_0$ introduce new randomly located fractures that change the scattering effect of the network on incident elastic waves. Previous work has shown that when the fracture lengths are distributed according to Gutenberg-Richter statistics, propagation of elastic waves incident on the network is exponentially dampted at oscillation frequencie ω greater than a mobility edge frequency ω_c, with damping lengthscale proportional to $(\omega - \omega_c)^{-1}$ [23]. Therefore, it is now postulated that resonant states of the τ-dependent 3D elastodynamic Green's function have eigenfrequencies $\omega > \omega_c(\tau)$, for some τ-dependent mobility edge frequency $\omega_c(\tau)$, and that these resonant states are

localized in 3D space with localization lengths $\mathscr{L}(\omega;\tau)$:

$$\mathscr{L}(\omega;\tau) \propto (\omega - \omega_c(\tau))^{-1}. \tag{21}$$

equating to rupture lengths of earthquakes occurring during seismic activation. Notably, this postulate suggests identifying $\omega - \omega_c(\tau)$ with the corner frequency of a seismic activation earthquake occurring at time τ, since the accepted seismic moment M_s scaling relation:

$$M_s \propto \mathscr{L}(\omega_0;\tau_0)^3, \tag{22}$$

together with relation (21) implies the scaling relation:

$$\omega - \omega_c(\tau) \propto M_s^{-1/3}, \tag{23}$$

that seismologists have observed in practice [1].

To quantify these statements with statistical mechanics formalism, it is now postulated that the statistical theory of energy levels applies to describe τ-dependent 3D resonant scattering data [15]. More specifically, it is postulated that increasing the set of fractures in a seismic activation region as $\tau \to \tau_0$ is analogous to increasing a disorder parameter W in a 3D disordered electronic model Hamiltonian from 0 to some critical value W_c, whereby the normalized level spacing distribution of 3D elastic resonant scattering states with real frequency component less than the elastic mobility edge $\omega_c(\tau)$ equates to the normalized level spacing distribution of non-localized electronic states [24]. In mathematical terms, this is the statement that the Wigner surmise distribution:

$$P_\beta(s) = c_0 \left(\frac{\pi s}{2}\right)^\beta e^{-\frac{1}{4}\beta\left(\frac{\pi s}{2}\right)^2 - \left(c_1 s - \frac{\beta}{4}\pi s\right)}, \tag{24}$$

with constants c_0 and c_1 determined by conditions:

$$\int_0^\infty P_\beta(s)ds = 1 \tag{25}$$

$$\int_0^\infty sP_\beta(s)ds = 1, \tag{26}$$

and a value of β between 0 and ∞ that depends on τ is the normalized level spacing distribution of 3D elastic resonant scattering states below the elastic mobility edge. Note that according to this postulate, the value $\beta(\tau)$ decreases monotonically to the value $\beta(\tau_0)$ as $\tau \to \tau_0$, since the normalized energy level spacings of non-localized electronic states at a conduction band center varies from delta function (i.e. uniform level spacing) to Poisson as the disorder parameter W is increased to W_c and the boundaries between localized and non-localized electronic states (i.e. mobility edges) on opposite sides of the band center converge together [16,36].

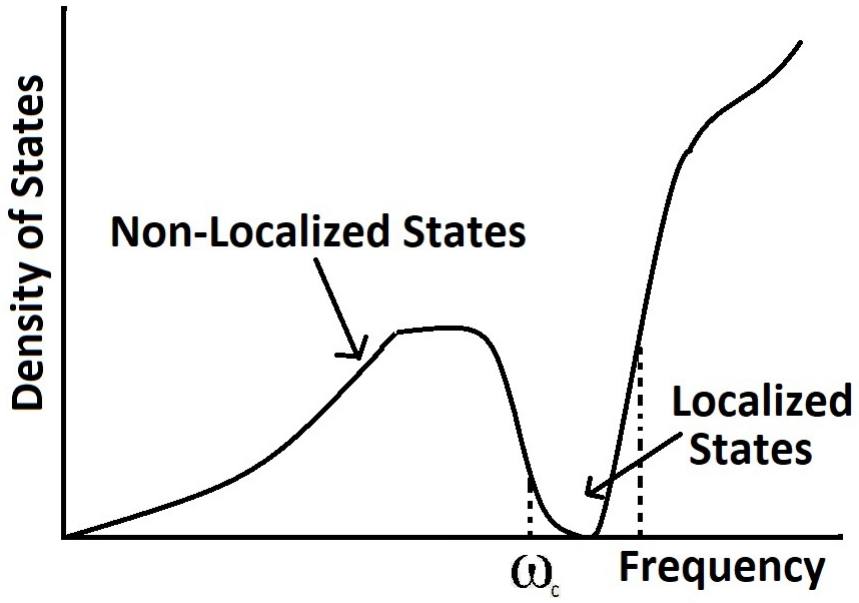

Fig. 5 Density of states diagram for light localization in a dielectric material [20]. Shaded region indicates frequencies associated with localized states.

3 Results

As initial evidence for the conjectured correspondence between seismic activation earthquakes and 3D resonant scattering states, assume that during the time interval $(\tau, \tau + \Delta\tau)$ the value of $\omega_c(\tau)$ is approximately constant, and that the density $\rho(\omega)$ of localized resonant scattering states in a neighborhood of the elastic mobility edge shown in Figure 5 satisfies:

$$\rho(\omega) \propto |\omega - \omega_c(\tau)|^{\beta(\tau)}. \tag{27}$$

Furthermore, assume that the decay time of each localized state is proportional to its localization length $\mathscr{L}(\omega;\tau)$, interpreted as the mean free path of acoustic scattering at frequency $\omega_c(\tau)$. Then, if localized states correspond to seismic activation earthquakes with rupture length proportional to $1/(\omega - \omega_c(\tau))$ occurring during the time interval $(\tau, \tau + \Delta\tau)$, the total number of earthquakes $\dot{N}_c$ with rupture length $\mathscr{L} > \mathscr{L}(\omega;\tau)$ occurring during the time interval satisfies:

$$\dot{N}_c \propto |\omega - \omega_c(\tau)|^{2+\beta(\tau)}, \tag{28}$$

from which it follows:

$$\log_{10}\dot{N}_c \approx \delta - (2+\beta(\tau))\log_{10}\mathscr{L}(\omega;\tau). \tag{29}$$

Therefore, given the relation between earthquake seismic moment and Richter magnitude:

$$M_{\mathscr{L}} = (\log_{10}(M_s) - 9)/1.5, \tag{30}$$

and the seismic moment relation:

$$M_s \propto \mathscr{L}(\omega;\tau_1)^3, \tag{31}$$

equation (29) is equivalent to the Gutenberg-Richter relation:

$$\log_{10}\dot{N}_c = \bar{\delta} - 0.5(2+\beta(\tau))M_{\mathscr{L}}. \tag{32}$$

This equation implies that when the density of localized resonant states is approximately constant so that $\beta(\tau) = 0$, the Gutenberg-Richter b-value is the physically reasonable value 1.0 ([18,20]).

If it is now supposed that rather than being proportional to localization length, the decay time of localized states is proportional to:

$$|\omega - \omega_c(\tau)|^{2/3}, \tag{33}$$

assuming critical slowing down of elastic waves propagating across disordered elastic material with osciallation frequency $\omega \approx \omega_c(\tau)$, it follows that relation (28) is replaced with relation:

$$\dot{N}_c \propto |\omega - \omega_c(\tau)|^{5/3+\beta(\tau)}, \tag{34}$$

and the Gutenberg-Richter b-value in equation (32) is approximately 0.83. Similarly, if the critical slowing down exponent in expression (33) is replaced with a value between 0 and 1, the Gutenberg-Richter b-value attains a value between 0.5 and 1.0. Therefore, if the density of localized elastic states $\rho(\omega)$ in Figure 5 is roughly constant except for a neighborhood of $\omega = \omega_c(\tau)$ where $\rho(\omega) \propto (\omega - \omega_c(\tau))^{\beta(\tau)}$, and the critical slowing down exponent decreases from 1 to a value between 0 and 1 as ω approaches $\omega_c(\tau)$ from above, it follows that the deviation from Gutenberg-Richter statistics shown in Figure 1 is accounted for by a correspondence between localized elastic states near the elastic mobility edge and seismic activation earthquakes.

Having provided initial evidence that Wigner surmise distributions are relevant to accounting for deviation of earthquake occurrence statistics from Gutenberg-Richter statistics during seismic activation, it is now further conjectured, in accordance with previous statistical physics models of seismic activation, that $\beta(\tau)$ can be regarded as a parameter in a τ-dependent 2D Coulomb gas statistical physics model whose parameters at different values of τ are related by renormalization group flow [10,3,9]. A phase diagram of a 2D Coulomb gas with a renormalization group flow indicated by arrows is shown in Figure 6. In this diagram, different vaues of the flow coordinate 't' equate to $\beta(\tau)$ at different values of τ in such a way that $\beta(\tau_0)$ is the horizontal coordinate of a point of tangency between two of the Ford circles. It should be noted that this phase diagram corresponds to the $M = 1$ description of a more general 2D Coulomb gas statistical physics model defined by a field theory with M complex fields ϕ whose domain of definition is a 2D complex plane, and whose amplitudes quantify the density of resonant scattering frequencies of a 3D differential operator at different complex frequencies [42,13,40].

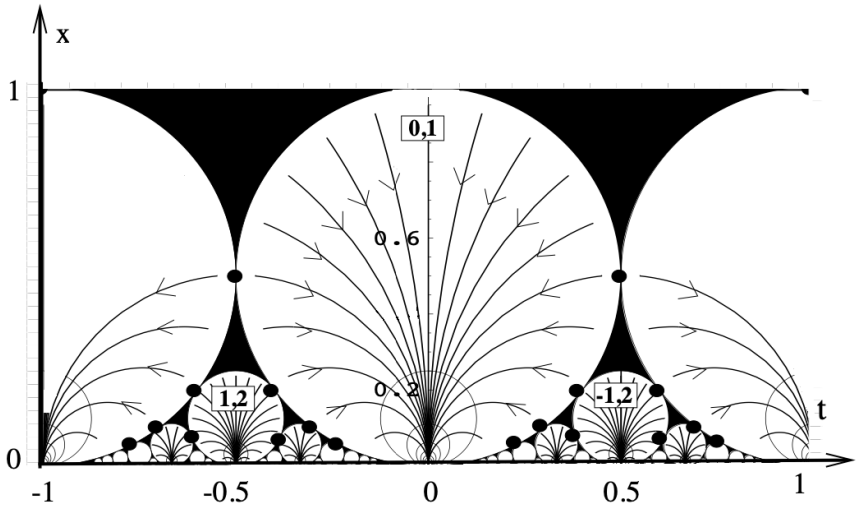

[h]

Fig. 6 Phase diagram of 2D Coulomb gas with renormalization group flow indicated by arrows and KT critical points identified by circle tangencies [10].

4 Discussion

Previous work has identified predicting the time of occurrence of major earthquakes as a possible application of statistical physics models of seismic activation, but this application has not yet been realized [6]. In more recent times, earthquake early warning algorithms such as FinDer and Virtual Seismologist have been developed which can in principle use previous earthquake occurrence statistics as input, and most recently, artificial intelligence algorithms such as QuakeGPT have been developed for predicting the occurrence of major earthquakes using seismic event records created with stochastic simulators as training data [5,33]. Therefore, a practical applied science goal for the statistical physics model presented in this article appears to be improving the predictive performance of one or more of these existing earthquake early warning algorithms by appropriately modifying their earthquake occurrence statistical inputs, acknowledging that preliminary tests of the model's validity against real seismic data must be passed before achieving this application objective can be considered a realistic possibility.

From a geophysical testing point of view, if it is true that the growth of unstable stress modes within the Earth during seismic activation are determined by statistical physics renormalization group flow mathematics, and, as a result, a nonlinear dynamical system of phase space dimension N characterizes the nucleation of shear stress in a seismic region preceding a major earthquake, a geophysical signal processing technique known as singular spectrum analysis should apply to determine this phase space dimension [7]. Therefore, it is suggested that coda wave interferometry measurements of relative changes in seismic surface wave and/or body wave velocity be performed between pairs of seismic stations in a seismic region over a duration of

time during which seismic activation is known to have occurred, and used as input to a time domain multichannel singular spectrum analysis algorithm [26]. The number of channels of this algorithm would equate to the number of station pairs, and the number of singular values output by the algorithm in different time windows preceding occurrence of a major earthquake should provide some indication of a finite value for N if the statistical physics model of seismic activation is correct in principle. With reference to previous geophysical application of singular spectrum analysis, performed in the frequency domain, the signal processing algorithm suggested here is different in that it should be carried out in the time domain τ rather than the frequency domain [34].

In conclusion, work towards improving current earthquake early warning systems can proceed in two directions. Firstly, as an initial check on whether or not the statistical physics modelling approach presented here could be of practical utility, work can be done to determine whether or not changes of the Earth's elastic velocity model preceding major earthquakes, as determined by coda wave interferometry, can be processed to extract an integer identifiable as the phase space dimension of a nonlinear dynamical system. Secondly, work can be done to elaborate upon the statistical physics mathematical model of seismic activation presented in this article to determine other tests of its scientific validity and potential for practical application.

References

1. Aki K, 1967. Scaling law of seismic spectrum, J. geophys. Res., 72, 1217–1231
2. Aktosun T, Demontis F, F Van der Mee C. Exact solutions to the sine-Gordon equation. Journal of Mathematical Physics. 51(12)
3. Balog I, Carpentier D, Fedorenko AA. Disorder-driven quantum transition in relativistic semimetals: functional renormalization via the porous medium equation. Physical review letters. 2018 121(16):166402
4. Ben-Zion Y, Lyakhovsky V (2002) Accelerated seismic release and related aspects of seismicity patterns on earthquake faults. Earthquake processes: Physical modelling, numerical simulation and data analysis Part II :2385–2412
5. Böse M, Andrews J, Hartog R, Felizardo C. Performance and next-generation development of the finite-fault rupture detector (FinDer) within the United States West Coast ShakeAlert warning system. Bulletin of the Seismological Society of America. 2023 Apr 1;113(2):648–63
6. Bowman D, Ouillon G, Sammis C, Sornette A, Sornette D (1998) An observational test of the critical earthquake concept. Journal of Geophysical Research: Solid Earth 103(B10):24359–24372
7. Broomhead D S, King G P (1986) Extracting qualitative dynamics from experimental data. Physica D: Nonlinear Phenomena 20(2-3):217–236
8. Bykov V G (2001) Solitary waves on a crustal fault. Volcanology and Seismology 22(6):651–661.
9. Carlson J M, Langer J S, Shaw B E (1994) Dynamics of earthquake faults. Reviews of Modern Physics 66(2):657
10. Carpentier D (1999) Renormalization of modular invariant Coulomb gas and sine-Gordon theories, and the quantum Hall flow diagram. Journal of Physics A: Mathematical and General 32(21):3865
11. Chen CC. Accelerating seismicity of moderate-size earthquakes before the 1999 Chi-Chi, Taiwan, earthquake: Testing time-prediction of the self-organizing spinodal model of earthquakes. Geophysical Journal International. 2003 155(1):F1-5
12. Cooper NR, Halperin BI, Hu CK, Ruzin IM (1997). Statistical properties of the low-temperature conductance peak heights for Corbino disks in the quantum Hall regime. Physical Review B 55(7):4551
13. Dubrovin B, Yang D (2020) Matrix resolvent and the discrete KdV hierarchy. Communications in Mathematical Physics 377:1823–1852
14. Dyatlov S, Zworski M (2019) Mathematical theory of scattering resonances, volume 200. American Mathematical Soc.
15. Dyson FJ, Mehta ML (1963) Statistical theory of the energy levels of complex systems. iv. Journal of Mathematical Physics 4(5):701–712
16. Hofstetter E, Schreiber M (1993) Statistical properties of the eigenvalue spectrum of the three-dimensional Anderson Hamiltonian. Physical Review B 48(23):16979
17. Imada M, Fujimori A, Tokura Y (1998) Metal-insulator transitions. Reviews of modern physics 70(4): 1039.
18. Ito R, Kaneko Y (2023). Physical Mechanism for a Temporal Decrease of the Gutenberg-Richter b-Value Prior to a Large Earthquake. Journal of Geophysical Research: Solid Earth 128(12):e2023JB027413
19. Jensen HJ (2003) Lecture Notes on Kosterlitz-Thouless Transition in the XY Model. Imperial College Lectures 9
20. John S. Localization of light. Physics Today. 1991 May 1;44(5):32–40.
21. Johnston AC, Kanter LR, Coppersmith KJ, Cornell CA (1994) The earthquakes of stable continental regions. volume 1, assessment of large earthquake potential, final report. Electric Power Research Inst.(EPRI), Palo Alto, CA (United States)
22. Khan BA, Chatterjee S, Sekh GA, Talukdar B (2020) Integrable systems: From the inverse spectral transform to zero curvature condition. arXiv preprint arXiv:2012.03456
23. Lei Q, Sornette D (2022) Anderson localization and reentrant delocalization of tensorial elastic waves in two-dimensional fractured media. Europhys. Letters 136(3): 1–7
24. Markos P (2006) Numerical analysis of the Anderson localization. arXiv preprint cond-mat/0609580
25. Md BY, Giurgiutiu V (2016) Using the gauge condition to simplify the elastodynamic analysis of guided wave propagation. Incas Bulletin. 8(3):11.
26. Merrill RJ, Bostock MG, Peacock SM, Chapman DS (2023) Optimal multichannel stretch factors for estimating changes in seismic velocity: Application to the 2012 M_w 7.8 Haida Gwaii earthquake. Bulletin of the Seismological Society of America 113(3):1077–1090

27. Newman WI, Turcotte DL, Gabrielov AM (1995) Log-periodic behavior of a hierarchical failure model with applications to precursory seismic activation. Physical Review E 52(5):4827
28. Papazachos C, Papazachos B (2001) Precursory accelerated Benioff strain in the Aegean area
29. Reches ZE (1999) Mechanisms of slip nucleation during earthquakes. Earth and Planetary Science Letters. Jul 30;170(4):475–86
30. Ruelle D, Takens F (1971) On the nature of turbulence. Les rencontres physiciens-mathématiciens de Strasbourg-RCP25 12:1–44.
31. Rundle JB, Klein W, Turcotte DL, Malamud BD (2001) Precursory seismic activation and critical-point phenomena. Microscopic and Macroscopic Simulation: Towards Predictive Modelling of the Earthquake Process 2165–2182
32. Rundle JB, Turcotte DL, Shcherbakov R, Klein W, Sammis C (2003) Statistical physics approach to understanding the multiscale dynamics of earthquake fault systems. Reviews of Geophysics 41(4)
33. Rundle JB, Fox G, Donnellan A, Ludwig IG (2024) Nowcasting Earthquakes with QuakeGPT: Methods and First Results. arXiv e-prints. 2024 Jun:arXiv-2406
34. Sacchi M (2009) FX singular spectrum analysis. Cspg Cseg Cwls Convention 392–395
35. Saleur H, Sammis C, Sornette D (1996) Renormalization group theory of earthquakes. Nonlinear Processes in Geophysics 3(2):102–109
36. Soerensen M, Schneider T (1991) Level-spacing statistics for the Anderson model in one and two dimensions. Physik B Condensed Matter 82(1):115–119
37. Sornette D (1989) Acoustic waves in random media: II Coherent effects and strong disorder regime, Acustica 67(4):251–265
38. Takahashi DA (2023) Multi-soliton solutions of the sine-Gordon equation with elliptic-function background. arXiv preprint arXiv:2301.08705. 2023 Jan 20.
39. Tzanis A, Vllianatos F (2003) Distributed power-law seismicity changes and crustal deformation in the SW Hellenic ARC. Natural Hazards and Earth System Sciences 3(3/4):179–195
40. Varchenko A (1990) Multidimensional hypergeometric functions in conformal field theory, algebraic K-theory, algebraic geometry. In Proceedings of the International Congress of Mathematicians 1:281–300
41. E.A. Zabolotskaya, Y.A. Ilinskii, T.A. Hay, M.F. Hamilton. *Green's functions for a volume source in an elastic half-space. The Journal of the Acoustical Society of America. 2012 Mar 1;131(3):1831-42.*
42. Zabrodin A (2010) Canonical and grand canonical partition functions of Dyson gases as tau-functions of integrable hierarchies and their fermionic realization. Complex Analysis and Operator Theory 4:497–514
43. Zuo Z, Yin S, Cao X, Zhong F (2021) Scaling theory of the Kosterlitz-Thouless phase transition. Physical Review B 104(21):214108